INTERNATIONAL JOURNAL FOR NUMERICAL METHODS IN FLUIDS
Int. J. Numer. Meth. Fluids 2002; **39**:763–781 (DOI: 10.1002/fld.328)

Embedded turbulence model in numerical methods for hyperbolic conservation laws

D. Drikakis*

Queen Mary, University of London, Department of Engineering, London E1 4NS, U.K.

SUMMARY

The paper describes the use of numerical methods for hyperbolic conservation laws as an *embedded turbulence modelling* approach. Different Godunov-type schemes are utilized in computations of Burgers' turbulence and a two-dimensional mixing layer. The schemes include a total variation diminishing, characteristic-based scheme which is developed in this paper using the flux limiter approach. The embedded turbulence modelling property of the above methods is demonstrated through coarsely resolved large eddy simulations with and without subgrid scale models. Copyright © 2002 John Wiley & Sons, Ltd.

KEY WORDS: turbulence; hyperbolic conservation laws; total variation diminishing; large eddy simulation; Godunov methods; unsteady flows

1. INTRODUCTION

In large eddy simulation (LES) all scales larger than the filter scale are computed via a modified (filtered) set of the Navier–Stokes equations while all scales smaller than the filter scale (approximately the grid size) are modelled using a subgrid scale model (SGS). Numerical accuracy presents a major challenge in LES, especially in coarsely resolved computations.

Previous studies [1–9] have shown that high-resolution (non-oscillatory) advection methods can represent the effects of the unresolved scales of motion in computations of turbulent flows without using a SGS model. Following Harten's definition [10], we classify as high resolution methods those with the following properties: (i) provide at least second-order of accuracy in smooth areas of the flow, (ii) produce numerical solutions (relatively) free from spurious oscillations, and (iii) in the case of discontinuities, the number of grid points in the transition zone containing the shock wave is smaller in comparison with that of first-order monotone methods. Godunov-type schemes belong to this family of methods.

Consider the system of hyperbolic conservation laws

$$\frac{\partial U}{\partial t} + \frac{\partial E(U)}{\partial x} = 0 \tag{1}$$

*Correspondence to: D. Drikakis, Department of Engineering, Queen Mary, University of London, Mile End Road, London E1 4NS, U.K.

Received October 2001
Revised December 2001

The advective flux derivative $\partial E/\partial x$ can be discretized at the centre of the control volume (i,j) using the values of the intercell fluxes, i.e. $\partial E/\partial x = (E_{i+1/2,j} - E_{i-1/2,j})/\Delta x$. Methods developed for solving hyperbolic conservation laws can be written in the general form of a Godunov-type intercell flux

$$E_{i+1/2} = \frac{1}{2}(E_L + E_R) - \frac{1}{2}|A|(U_R - U_L) \tag{2}$$

where $E_L = E_L(U_L)$ and $E_R = E_R(U_R)$ denote the left and right states of the flux, respectively, at the cell face. Similarly, U_L and U_R are the left and right states, respectively, of the vector U at the cell face. The second term in the right-hand-side (RHS) of Equation (2) is the wave-speed dependent term (WST), where A approximates $\partial E/\partial U$ (the entries of the Jacoby matrix, in general). The WST term is a function of the local wave speeds and flow data. It is essentially acting as a non-linear numerical viscosity that adjusts the amount of numerical dissipation locally, i.e. at the cell faces, in order to maintain monotonicity and conservation.

According to Godunov's theorem [11] (linear) monotone methods are at most first-order accurate. To obtain high-order of accuracy and avoid spurious oscillations one has to construct non-linear methods. Total Variation Diminishing (TVD) methods are the most prominent class of non-linear methods; a review of these methods can be found in Reference [12]. TVD methods can be constructed by using the concept of flux limiters [13–15]. According to this, the TVD flux can be defined by

$$E^{\mathrm{TVD}}_{i+1/2} = E^{\mathrm{LO}}_{i+1/2} + \psi(E^{\mathrm{HI}}_{i+1/2} - E^{\mathrm{LO}}_{i+1/2}) \tag{3}$$

where $E^{\mathrm{HI}}_{i+1/2}$ is a high-order flux (at least second-order), $E^{\mathrm{LO}}_{i+1/2}$ is the flux of a first-order monotone scheme and ψ is a flux limiter function. The low and high-order fluxes can be written in the form of Equation (2). The limiter acts on the numerical viscosity (WST terms) as a non-linear switch that is used to preserve monotonicity. It essentially provides a numerical mechanism for adapting the choice of numerical method based upon the behaviour of the local flow gradients. This results in non-linear numerical viscosity that is dynamically adapted during the computation as function of the local data. Similar conclusions can be drawn by analysing the non-linear truncation error arising from the discretization of high-resolution methods [3, 4].

In this paper we develop a TVD scheme by combining a high-order (at least second-order) characteristic-based (CB) scheme [9, 16] and the first-order Lax-Friedrich flux [27] using the flux limiter approach. Computations of Burgers' turbulence* [17] as well as a two-dimensional mixing layer have been conducted using the CB and TVD-CB schemes with and without SGS models. The dynamic [18, 19] and structure-function [20] SGS models have been utilized for comparison purposes.

The paper is organized as follows. In Section 2 the TVD-characteristic-based scheme for solving the incompressible Navier–Stokes equations is presented. In Section 3 results from computations of Burgers' turbulence and a two-dimensional mixing-layer using different Godunov-type schemes with and without SGS models are discussed. The conclusions drawn from the present work are summarized in Section 4.

*This can be considered as the one-dimensional analogue of the Navier–Stokes turbulence.

2. TVD SCHEME FOR INCOMPRESSIBLE FLOWS

2.1. Numerical framework

To take full advantage of the Godunov methods designed for hyperbolic conservation laws, the incompressible Navier–Stokes equations are cast in a compressible format by means of the artificial-compressibility approach [21]. The classical formulation of Chorin [21], suitable for steady-state problems, is extended to transient flows via dual-time stepping [9, 22, 23]

$$\frac{1}{\beta}\frac{\partial p}{\partial \tau} + \frac{\partial u_j}{\partial x_j} = 0 \tag{4}$$

$$\frac{\partial u_i}{\partial \tau} + \frac{\partial}{\partial x_j}(u_i u_j + p\delta_{ij}) = -\frac{\partial u_i}{\partial t} + \frac{1}{Re}\Delta u_i \tag{5}$$

where β is the artificial compressibility parameter, $u_i = (u, v, w)$ are the velocity components, p is the pressure, and Re is the Reynolds number; the indices $i, j = 1, 2, 3$ refer to the space co-ordinates x, y, z. The above system provides a coupling of the equations with respect to the pseudotime τ, at each real time step t. The attenuation forcing $-\partial u_i/\partial t$ on the RHS of the momentum equation damps the flow divergence to zero at the rate $\alpha \equiv (\Delta t)^{-1}$. In the steady-state at $\tau = t + \Delta t$, all $\partial/\partial\tau$ terms vanish.

In the present model the default time integration with respect to τ employs a fourth-order Runge–Kutta scheme [24] (selected, primarily, for the optimum performance on non-uniform grids) while a non-linear multigrid method [25] is used to accelerate the convergence towards the steady state. The viscous terms are discretized by standard central differences.

Godunov-type schemes are employed for discretizing the three advective fluxes of the system Equations (4)–(5). In Cartesian co-ordinates the advective flux associated with the derivative in x-direction is written in matrix form as

$$E \equiv \begin{pmatrix} \beta u \\ u^2 + p \\ uv \\ uw \end{pmatrix} \tag{6}$$

The matrix of primitive variables is $U = (p, u, v, w)^T$. The Jacobian of this flux has eigenvalues: $\lambda_0 = u,\ \lambda_1 = \lambda_0 + \tilde{s},\ \lambda_2 = \lambda_0 - \tilde{s}$, where $\tilde{s} = \sqrt{\lambda_0^2 + \beta}$.

2.2. TVD formulation

The TVD flux is defined by Equation (3). We have employed the Lax–Friedrichs flux [27] as a low-order flux

$$E^{\mathrm{LO}}_{i+1/2} = \frac{1}{2}(E_i + E_{i+1}) - \frac{1}{2}\frac{\Delta x}{\Delta t}(U_{i+1} - U_i) \tag{7}$$

The CB scheme of [9, 16] has been employed as a high-order flux.

The CB scheme computes the advective flux in a sequence of reconstruction steps:

1. For each characteristic (denoted by $l=0,1,2$), we calculate the variables U_l using an upwind Godunov scheme

$$U_l=\frac{1}{2}[(1+\text{sign}(\lambda_l))U_L+(1-\text{sign}(\lambda_l))U_R] \tag{8}$$

where

$$\text{sign}(\lambda_l)=\begin{cases}-1 & \text{for } \lambda_l<0\\ 1 & \text{for } \lambda_l>0\end{cases} \tag{9}$$

The left, U_L, and right, U_R, states of the primitive variables are calculated by high-order interpolation from the variables in the neighbouring cells, for example,

$$U_L=\frac{1}{6}(5U_i-U_{i-1}+2U_{i+1}),\qquad U_R=\frac{1}{6}(5U_{i+1}-U_{i+2}+2U_i) \tag{10}$$

Note that the interpolation in Equation (10) is not third-order-accurate *per se*, but it assures third-order accuracy of the term (U_R-U_L) in Equation (2) [16].

2. Using U_l, we calculate the new variables $\tilde{U}$ (*reconstructed variables*). The variables $\tilde{U}$ associated with the advective flux E (in Cartesian co-ordinates[†]) are given by

$$\tilde{U}=\begin{pmatrix}\tilde{p}\\ \tilde{u}\\ \tilde{v}\\ \tilde{w}\end{pmatrix}=\frac{1}{2\tilde{s}}\begin{pmatrix}\lambda_1\lambda_2(u_2-u_1)+\lambda_1 p_2-\lambda_2 p_1\\ p_1-p_2+\lambda_1 u_1-\lambda_2 u_2\\ 2\tilde{s}v_0\\ 2\tilde{s}w_0\end{pmatrix} \tag{11}$$

3. The advective flux, E^{CB}, for the CB scheme is calculated using the variables $\tilde{U}$, i.e. $E^{\text{CB}}=E(\tilde{U})$.

For non-linear and multi-dimensional systems such as the Navier–Stokes equations it is not possible to derive the accuracy of Godunov-type schemes. For linear problems such as the linear advection equation $u_t+(au)_x=0$, where a is a constant, the accuracy can be derived by using Roe's theorem [12, 26]. The theorem states that any scheme written in the form

$$u_i^{n+1}=\sum_{k=-k_L}^{k_R}c_k u_{i+k}^n \tag{12}$$

is pth order accurate *in space and time* if

$$\sum_{k=-k_L}^{k_R}k^q c_k=(-\mathscr{C})^q,\quad 0\leqslant q\leqslant p \tag{13}$$

where k_L and k_R are two non-negative integers, c_k are scheme dependent coefficients, and $\mathscr{C}=a\Delta t/\Delta x$ is the Courant–Friedrichs–Lewy (CFL) number.

[†]The derivation of $\tilde{U}$ as function of U_l in generalized curvilinear co-ordinates can be found in References [16] and [9] for 2D and 3D problems, respectively.

Application of the above theorem in the case of the CB scheme[‡] shows that the CB scheme is first-, second-[§] and third-order accurate in both space and time when it is implemented in conjunction with the Euler, second-order TVD Runge–Kutta [24], and third-order TVD Runge–Kutta time-stepping schemes [24], respectively.

The TVD scheme based on the combination of the Lax–Friedrichs and CB schemes is hereafter referred to as 'TVD-CB'.

2.3. Flux limiters

To construct flux limiters for the TVD-CB scheme we employ the linear advection equation $u_t + f_x = 0$, where $f = au$. Using the upwind Godunov discretization defined by Equations (8) and (10), we write the high-order flux f^{HI} as

$$f^{\mathrm{HI}}_{i+1/2} = \beta_{-1} f_{i-1} + \beta_0 f_i + \beta_1 f_{i+1} + \beta_2 f_{i+2} \tag{14}$$

where $\beta_{-1} = -(1+s)/12$, $\beta_0 = (7+3s)/12$, $\beta_1 = (7-3s)/12$, $\beta_2 = -(1-s)/12$, and $s = \mathrm{sign}(a)$. We also write the low-order flux f^{LO} as

$$f^{\mathrm{LO}} = \alpha_0 f_i + \alpha_1 f_{i+1} \tag{15}$$

where for the Lax–Friedrich flux, $\alpha_0 = (1 + \mathscr{C})/2\mathscr{C}$ and $\alpha_1 = -(1 - \mathscr{C})/2\mathscr{C}$ ([12], p. 419). Using Equations (14) and (15), the TVD version (Equation (3)) of the flux f at the cell faces $i - 1/2$ and $i + 1/2$ is written

$$f^{\mathrm{TVD}}_{i+1/2} = \beta_{-1}\psi f_{i-1} + \beta_2 \psi f_{i+2} + [\alpha_0 + \psi(\beta_0 - \alpha_0)] f_i + [\alpha_1 + \psi(\beta_1 - \alpha_1)] f_{i+1} \tag{16}$$

$$f^{\mathrm{TVD}}_{i-1/2} = \beta_{-1}\psi f_{i-2} + \beta_2 \psi f_{i+1} + [\alpha_0 + \psi(\beta_0 - \alpha_0)] f_{i-1} + [\alpha_1 + \psi(\beta_1 - \alpha_1)] f_i \tag{17}$$

Using Equations (16) and (17) the discretized linear advection equation is written

$$u^{n+1}_i = u^n_i - C\Delta u_{i-1/2} + D\Delta u_{i+1/2} - E\Delta u_{i-3/2} + F\Delta u_{i+3/2} \tag{18}$$

where $\Delta u_{i-1/2} = u_i - u_{i-1}$; $\Delta u_{i+1/2} = u_{i+1} - u_i$; $\Delta u_{i-3/2} = u_{i-1} - u_{i-2}$; $\Delta u_{i+3/2} = u_{i+2} - u_{i+1}$; $C = \mathscr{C}[\alpha_0 + \psi(\beta_0 - \alpha_0)]$; $D = -\mathscr{C}[\alpha_1 + \psi(\beta_1 - \alpha_1)]$; $E = \mathscr{C}\beta_{-1}\psi$, and $F = -\mathscr{C}\beta_2\psi$.

To derive limiter functions such that the scheme will be TVD, we apply the data compatibility condition [12, 26]. Harten's theorem [10] can also be used for deriving flux limiters but the data compatibility condition is a stronger constraint [12].[¶] The data compatibility condition is expressed as follows

$$0 \leqslant \frac{u^{n+1}_i - u^n_i}{u^n_{i-s} - u^n_i} \leqslant 1 \tag{19}$$

[‡]Note that for the linear advection equation the CB scheme is obtained by applying only the first reconstruction step. This is equivalent to the extension of the original first-order Godunov method in conjunction with a longer computational stencil.

[§]The coefficients for second-order of accuracy are given in Appendix A.

[¶]Different approaches for building monotone schemes are also discussed in Reference [28].

For $a>0$ (a similar analysis can be applied for $a<0$), Equation (18) can be written as[‖]

$$\frac{u_i^{n+1}-u_i^n}{u_{i-1}^n-u_i^n}=C-\frac{D}{r}+\frac{E}{\tilde{r}} \tag{20}$$

where $r=\Delta u_{i-1/2}/\Delta u_{i+1/2}$ and $\tilde{r}=\Delta u_{i-1/2}/\Delta u_{i-3/2}$. Note that depending on the sign of a the ratio of upwind change r should be correctly interpreted, i.e.

$$r=\frac{\Delta_{upw}}{\Delta_{loc}}=\begin{cases}\dfrac{u_i^n-u_{i-1}^n}{u_{i+1}^n-u_i^n}, & a>0\\[2ex] \dfrac{u_{i+2}^n-u_{i+1}^n}{u_{i+1}^n-u_i^n}, & a<0\end{cases} \tag{21}$$

Equations (19) and (20) give

$$0\leqslant\mathscr{C}[\alpha_0+\psi(\beta_0-\alpha_0)]+\mathscr{C}[\alpha_1+\psi(\beta_1-\alpha_1)]\frac{1}{r}-\psi\frac{\mathscr{C}}{6\tilde{r}}\leqslant 1 \tag{22}$$

We impose a global constraint

$$\psi_B\leqslant\psi\leqslant\psi_T \tag{23}$$

where ψ_T and ψ_B are the top and bottom boundaries of the flux limiter, which are considered to be independent of r and $\tilde{r}$; Equation (23) gives

$$\begin{aligned}\mathscr{C}\left[\alpha_0+\psi_T\left(\beta_0-\alpha_0-\frac{1}{6\tilde{r}}\right)\right]&\leqslant\mathscr{C}\left[\alpha_0+\psi\left(\beta_0-\alpha_0-\frac{1}{6\tilde{r}}\right)\right]\\&\leqslant\mathscr{C}\left[\alpha_0+\psi_B\left(\beta_0-\alpha_0-\frac{1}{6\tilde{r}}\right)\right]\end{aligned} \tag{24}$$

assuming that $\beta_0-\alpha_0-1/6\tilde{r}\leqslant 0$ that is equivalent to

$$\tilde{r}=\frac{u_{i-1}-u_i}{u_{i-1}-u_{i-2}}<\frac{\mathscr{C}}{2\mathscr{C}-3} \tag{25}$$

For $\beta_0-\alpha_0-1/6\tilde{r}>0$ the analysis will be the same if in Equation (24) the terms ψ_B and ψ_T replace each other.

To satisfy Equations (22) and (24), the following inequality should be satisfied

$$\begin{aligned}-\mathscr{C}\left[\alpha_0+\psi_T\left(\beta_0-\alpha_0-\frac{1}{6\tilde{r}}\right)\right]&\leqslant\mathscr{C}[\alpha_1+\psi(\beta_1-\alpha_1)]\frac{1}{r}\\&\leqslant 1-\mathscr{C}\left[\alpha_0+\psi_B\left(\beta_0-\alpha_0-\frac{1}{6\tilde{r}}\right)\right]\end{aligned} \tag{26}$$

[‖]For $a>0$ E and F take the values $-\mathscr{C}\psi/6$ and 0, respectively.

Analysis of the left inequality gives

$$\psi = \begin{cases} \geqslant \psi_L & \text{for } r \geqslant 0 \\ \leqslant \psi_L & \text{for } r < 0 \end{cases} \tag{27}$$

where

$$\psi_L = \frac{1}{\beta_1 - \alpha_1}\left[-r\left(\alpha_0 + \psi_T\left(\beta_0 - \alpha_0 - \frac{1}{6\tilde{r}}\right)\right) - \alpha_1\right] \tag{28}$$

Analysis of the right inequality gives

$$\psi = \begin{cases} \leqslant \psi_R & \text{for } r \geqslant 0 \\ \geqslant \psi_R & \text{for } r < 0 \end{cases} \tag{29}$$

where

$$\psi_R = \frac{1}{\beta_1 - \alpha_1}\left[\frac{r}{\mathscr{C}} - r\left(\alpha_0 + \psi_B\left(\beta_0 - \alpha_0 - \frac{1}{6\tilde{r}}\right)\right) - \alpha_1\right] \tag{30}$$

Equations (28) and (30) are functions of the ratios r and $\tilde{r}$. For large flow gradients occurring within the stencil $i-1$, i and $i+1$, $\Delta u_{i-3/2} < \Delta u_{i+1/2}$ thus $r/\tilde{r} < 1$. As a result, $\psi_B r/\tilde{r}$ and $\psi_T r/\tilde{r}$ can be considered small compared to the rest terms in Equations (28) and (30) thus can be dropped. For Burgers' turbulence and the two-dimensional mixing layer considered in this work, it was found that these terms do not affect the accuracy of the computations. Alternatively, one can attempt to approximate $\psi_B r/\tilde{r}$ and $\psi_T r/\tilde{r}$ as functions of the ratio r, but this is beyond the scope of the present paper.

We substitute β_0, β_1, α_0 and α_1 into Equations (28) and (30) and obtain

$$\psi_R = \frac{3(1-\mathscr{C}) - (2\mathscr{C}-3)\psi_B}{3-\mathscr{C}} r + \frac{3(1-\mathscr{C})}{3-\mathscr{C}} \tag{31}$$

$$\psi_L = -\frac{3 + 3\mathscr{C} + (2\mathscr{C}-3)\psi_T}{3-\mathscr{C}} r + \frac{3(1-\mathscr{C})}{3-\mathscr{C}} \tag{32}$$

The construction of the limiter functions ψ_L and ψ_R is completed after defining the top and bottom boundaries of the flux limiter. Concerning this point, there is a flexibility in constructing different TVD schemes depending on the definitions of ψ_B and ψ_T.

For $\psi_B = 0$ and $\psi_T = 3(1+\mathscr{C})/(3-2\mathscr{C})$, we obtain

$$\psi_R = \frac{3(1-\mathscr{C})}{3-\mathscr{C}}(r+1) \tag{33}$$

$$\psi_L = \frac{3(1-\mathscr{C})}{3-\mathscr{C}} \tag{34}$$

Using Equations (33) and (34), we define the flux limiter (hereafter referred to as *CB-limiter*)

$$\psi = \begin{cases} \dfrac{3(1-\mathscr{C})}{3-\mathscr{C}} & \text{if } r \leqslant 0 \\ \dfrac{3(1-\mathscr{C})}{3-\mathscr{C}}(r+1) & \text{if } 0 \leqslant r \leqslant \dfrac{\mathscr{C}(7-3\mathscr{C})}{(3-2\mathscr{C})(1-\mathscr{C})} \\ \dfrac{3(1+\mathscr{C})}{3-2\mathscr{C}} & \text{if } r > \dfrac{\mathscr{C}(7-3\mathscr{C})}{(3-2\mathscr{C})(1-\mathscr{C})} \end{cases} \tag{35}$$

In the literature, one can find limiters for TVD schemes designed for the compressible Euler equations. An example is the the Superbee limiter [15]

$$\psi^{sb} = \begin{cases} 0 & r \leqslant 0 \\ 2r & 0 \leqslant r \leqslant \frac{1}{2} \\ 1 & \frac{1}{2} \leqslant r \leqslant 1 \\ \min[2, \psi_g + (1-\psi_g)r] & r > 1 \end{cases} \tag{36}$$

where $\psi_g = (1-\mathscr{C})/(1+\mathscr{C})$. Although the flux limiter should be designed for the numerical scheme in question, we have found that converged solutions can also be obtained by implementing limiters developed for other schemes. Therefore, in addition to the CB-limiter we have also implemented the TVD-CB scheme in conjunction with the Superbee limiter; the effects on the accuracy of the computations are discussed in Section 3.

To calculate any of the flux limiter functions we use the following procedure [12]:

- The ratios r^L and r^R are calculated at the cell faces

$$r^L_{i+\frac{1}{2}} = \frac{\Delta u_{i-1/2}}{\Delta u_{i+1/2}}, \quad r^R_{i+\frac{1}{2}} = \frac{\Delta u_{i+3/2}}{\Delta u_{i+1/2}} \tag{37}$$

  where $\Delta(\cdot)$ denotes u-velocity differences at the cell faces.**
- Then we compute the flux limiter as

$$\psi = \min(\psi(r^L_{i+1/2}), \psi(r^R_{i+1/2})) \tag{38}$$

The flux limiter ψ is applied to all flux components.

3. NUMERICAL EXPERIMENTS

We have employed the Burgers' equation

$$\frac{\partial u}{\partial t} + u\frac{\partial u}{\partial x} = \nu\frac{\partial^2 u}{\partial x^2} \tag{39}$$

**The pressure or any velocity component can be used to calculate the intercell slopes. For the mixing layer flow considered in this paper, we have found that the velocity u is the most appropriate variable.

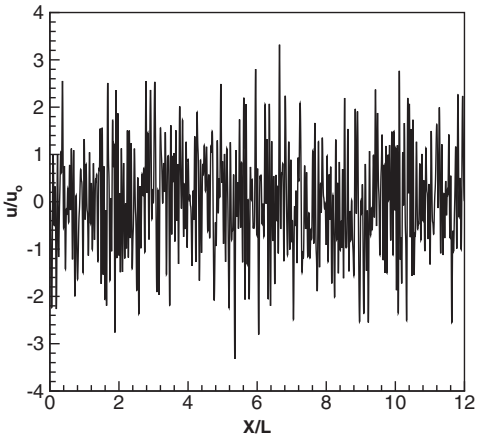

Figure 1. Initial condition for Burgers' problem of turbulence.

subject to periodic boundary conditions

$$u(x,t) = u(x+l,t), \quad 0 \leqslant x \leqslant l \tag{40}$$

and a random initial condition for the velocity u (Figure 1). The wave spectrum of the velocity profile of Figure 1 has a maximum at $\log(k) = 1.283$, where k is the wavenumber. We therefore define a characteristic length scale $L_o = 1/\log^{-1}(1.283)L = 0.052L$ (L is an arbitrary unit of length; here $L = 1$), and a characteristic velocity u_o as the root mean square of the initial condition. The viscosity v can then be defined by $v = (L_o u_o)/Re$, where Re is the Reynolds number. In Equation (40) we have defined the length of the domain as $l = 12L = 12$. Our computations have been conducted for $Re = 6000$.

We perform spatial filtering [29] of Equation (39) and obtain

$$\frac{\partial \bar{u}}{\partial t} + \frac{1}{2}\frac{\partial \bar{u}^2}{\partial x} = v\frac{\partial^2 \bar{u}}{\partial x^2} - \frac{1}{2}\frac{\partial \tau}{\partial x} \tag{41}$$

where $\tau = \overline{u^2} - \bar{u}^2$ is the subgrid-scale (SGS) stress. The filtered velocity $\bar{u}$ is defined by

$$\bar{u}(x,t) = \int_{-\infty}^{+\infty} G(x-x')u(x',t)\,\mathrm{d}x' \tag{42}$$

where G is the filter function.

We have carried out a series of computations for Burgers' turbulence using the CB and TVD-CB schemes with and without SGS models. To assess the accuracy of coarsely resolved computations we have initially carried out a computation using a very fine grid (9000 grid points) and a very small time step ($\Delta t = 0.0001$). The obtained solution (henceforth labelled DNS or 'Direct Numerical Solution') is grid and time-step independent and can, therefore, be considered as the exact solution.

The coarsely resolved computations have been carried out using 700 grid points and 100 time steps. In the numerical experiments we have employed the following schemes and SGS models:††

- The CB scheme without a SGS model (solution labelled 'CB').
- The TVD-CB scheme without a SGS model (solution labelled 'TVD-CB').
- The CB scheme in conjunction with the modified version [18] of the dynamic SGS model [19] (solution labelled 'CB-D').
- The CB scheme in conjunction with the structure-function SGS model [20] (solution labelled 'CB-SF').
- The TVD-CB scheme in conjunction with the structure-function SGS model (solution labelled 'TVD-CB & SF-Model').

In Figure 2 we present the results for the kurtosis distribution. The computations reveal that the use of a SGS model does not necessarily improve the results, e.g. compare the CB solutions with and without the dynamic SGS model, as well as the TVD-CB solutions with and without the structure-function SGS model. Implementation of the SGS models seems to improve the results in certain time intervals of the computation, but the results deteriorate in other time intervals. The best result for the averaged kurtosis (Table I) is obtained by the TVD-CB scheme without a SGS model.

Computation of Burgers' turbulence leads to an energy spectrum $E(k) \propto k^{-2}$ [17]. The wave spectra for all schemes and models are shown in Figure 3.

In all spectra curves we have applied smoothing in order to reduce 'noise' and thus make the data presentable. For the CB scheme with and without the dynamic SGS model the results look very similar and in both cases the spectra predictions are inferior than those obtained by this scheme in conjunction with the structure-function SGS model. The TVD-CB scheme predicts overall the best spectra behaviour. Similar to the kurtosis results, the combination of the TVD-CB scheme with the structure-function SGS model does not improve the spectra results.

Further, we have carried out numerical experiments for a two-dimensional temporal mixing layer defined by a velocity profile $u(y) = \tanh(y)$, where $u(y)$ and y are made dimensionless by the free-stream velocity, U, and half of the initial vorticity thickness, $\delta/2$ (δ is the initial vorticity thickness). The dimensionless time is $t = 2TU/\delta$, where T is the time with dimensions. The Reynolds number is defined as $Re = 0.5U\delta/v$, where v is the kinematic viscosity; our numerical experiments have been conducted for $Re = 200$. We solve the equations in a square domain $[0, L] \times [-L/2, L/2]$, imposing periodic boundary conditions in the x-direction and free slip walls in the y-direction, i.e. $v = (\partial p/\partial y) = (\partial u/\partial y) = 0$ at the boundaries. Similarly with previous studies [31, 32], we add to the basic flow a sine wave superimposed by a solenoidal white-noise perturbation of small amplitude. The initial conditions for u and v are given by

$$u_{in} = u(y) + d_1 f(x, y) \exp(-y^2) + d_2 \sin(\pi x/\lambda_u) \tag{43}$$

$$v_{in} = d_2 \sin(\pi x/\lambda_u) \tag{44}$$

†† For modelling $\tau = \overline{u^2} - \bar{u}^2$.

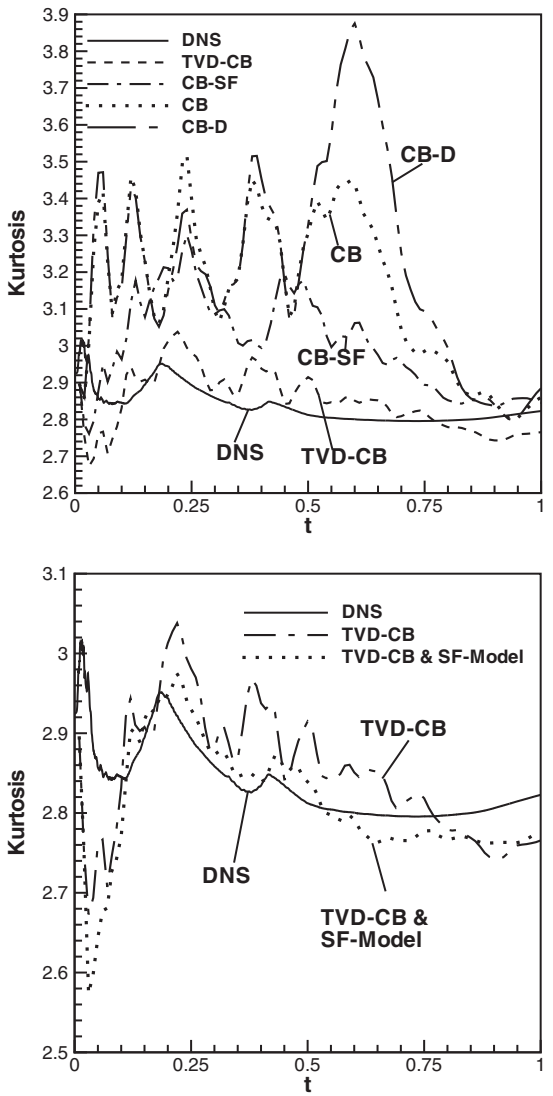

Figure 2. Kurtosis distributions: the upper plot compares the DNS results with the corresponding results obtained by the CB scheme without a SGS model (solution labelled 'CB'), TVD-CB scheme without a SGS model (solution labelled 'TVD-CB'), CB scheme in conjunction with the structure-function SGS model (solution labelled 'CB-SF'), and CB in conjunction with the dynamic SGS model (solution labelled 'CB-D'); the lower plot compares the results obtained by the TVD-CB scheme with the structure-function SGS model (solution labelled 'TVD-CB & SF-Model') and without it (solution labelled 'TVD-CB').

where $f(x, y)$ is the perturbation function (having values in the interval $[0, 1]$) and λ_u is the most unstable wavelength which, according to the theory [33], is defined as $\lambda_u = 7\delta$; in our experiments $d_1 = 0.1$ and $d_2 = 0.05$. The length of the computational domain should be taken

Table I. Averaged kurtosis for different Godunov-type schemes and SGS models.

Method	Averaged kurtosis
DNS	2.8371
TVD-CB & SF-Model	2.8131
TVD-CB	2.8487
CB	3.1515
CB-SF	3.
CB-D	3.2192

equal to $L_n/(0.5\delta) = 14n$ (dimensionless) for obtaining n Kelvin–Helmoltz vortices [32]. In the present work, we have conducted computations for $n = 2$. Two vortices are initially formed and later merge to form one large vortex (Figure 4).

Computations have been conducted on a sequence of increasingly finer grids containing 64×64, 128×128, 256×256 and 512×512 grid points, using different Godunov-type schemes without a SGS model. The results on 256×256 and 512×512 grids were almost identical: the differences in the velocity values were less than 1%. Hence, the results on the 256×256 grid are referred to as the corresponding '2D DNS'.

In addition to the CB scheme, we have also employed, for comparison purposes, the Einfeldt's HLLE Godunov-type scheme [30] (see Appendix B). Figure 5 shows the results for the CB and HLLE schemes on the 64×64 grid. The same contour values have been plotted for both schemes at two different time instants. The HLLE scheme results in thicker—more diffusive—shear layers at $t = 4$; additionally, the details of the core of the vortex at $t = 14$ are missing. The CB scheme provides very similar results on the 64×64 and 128×128 grids. The isovorticity contours for the TVD-CB scheme (not plotted here) were very similar to those obtained by the CB scheme.

Comparisons of the various solutions can be obtained on the basis of the vorticity thickness. This is defined as $\delta = 2U/(\mathrm{d}\bar{u}/\mathrm{d}y)_{\max}$, where the 'bar' denotes an average in the x-direction. In Figure 6 we plot the growth of vorticity thickness for all schemes, while in Figure 7 we compare the results obtained by the TVD-CB scheme with and without the structure-function SGS model.

The results show the following:

1. The particular details of the discretization even for schemes belonging to the same class of methods, Godunov-type in the present case, have significant impact on the accuracy of coarsely resolved computations. Specifically, the CB scheme provides better results than the HLLE scheme on the 64×64 grid, while the TVD-CB scheme is slightly less diffusive than the CB scheme.
2. The solution without the SGS model is better than the one with it (Figure 7).
3. The design details of the flux limiter also affect the accuracy. For example, the Superbee limiter gives inferior results than the CB limiter, especially for the peak values of the vorticity thickness. This can be attributed to the fact that the Superbee limiter has not been designed for the case of the CB scheme.

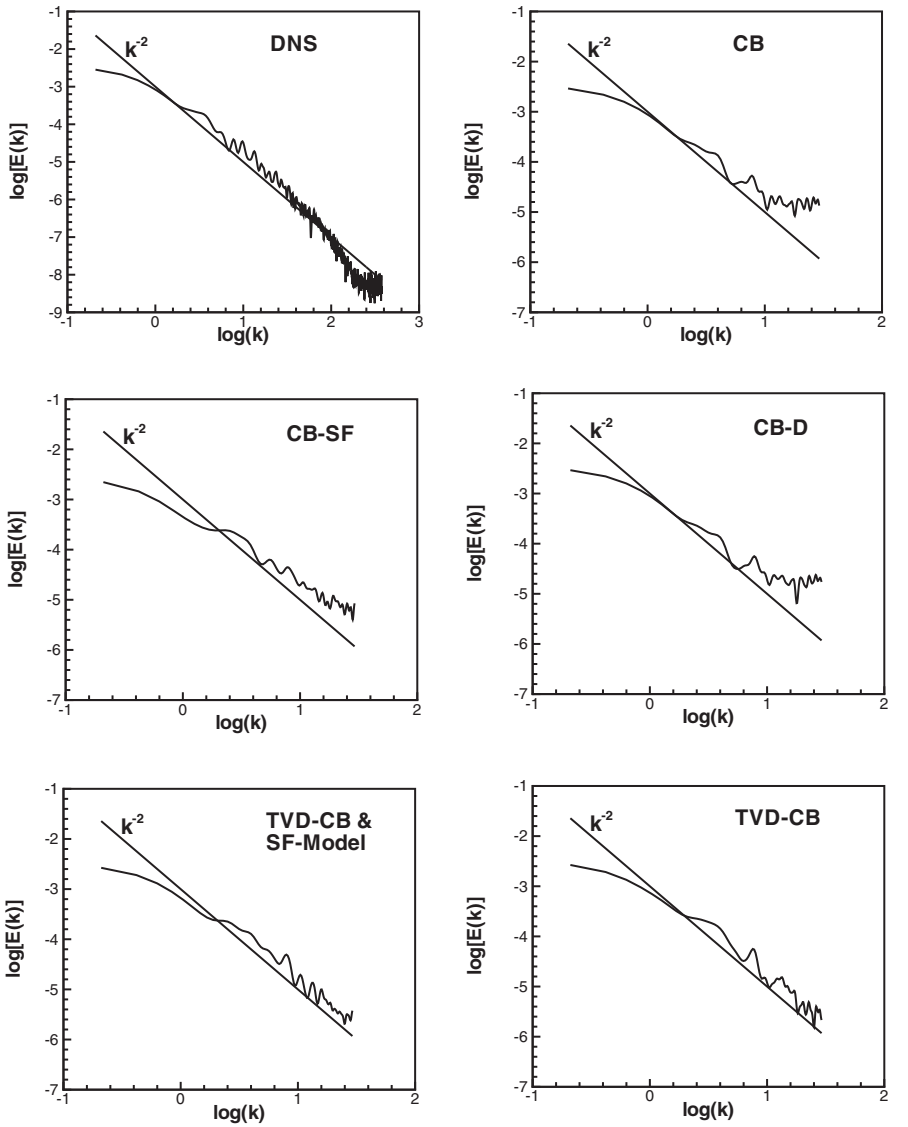

Figure 3. Wavenumber spectra for Burgers' turbulence as obtained by: DNS, CB, CB-SF, CB-D, TVD-CB & SF-Model, and TVD-CB schemes (see caption of Figure 2 and the text for description of different schemes and models).

In Table II, the total number of multigrid (MG) cycles required by the non-linear multigrid method [25] in conjunction with different Godunov-type schemes, is reported. The table shows that: (i) the efficiency of the computations depends strongly on the numerical scheme employed, (ii) the TVD-CB scheme is faster than the HLLE and CB schemes, and (iii) the non-linear MG method requires less MG sweeps as the grid is further refined.

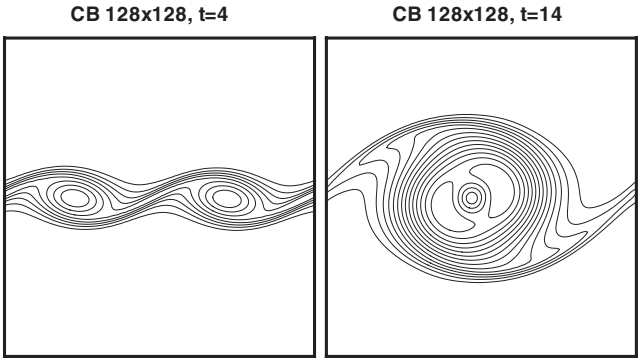

Figure 4. Isovorticity contours on the 128×128 grid, at $t = 4$ (left plot) and $t = 14$ (right plot).

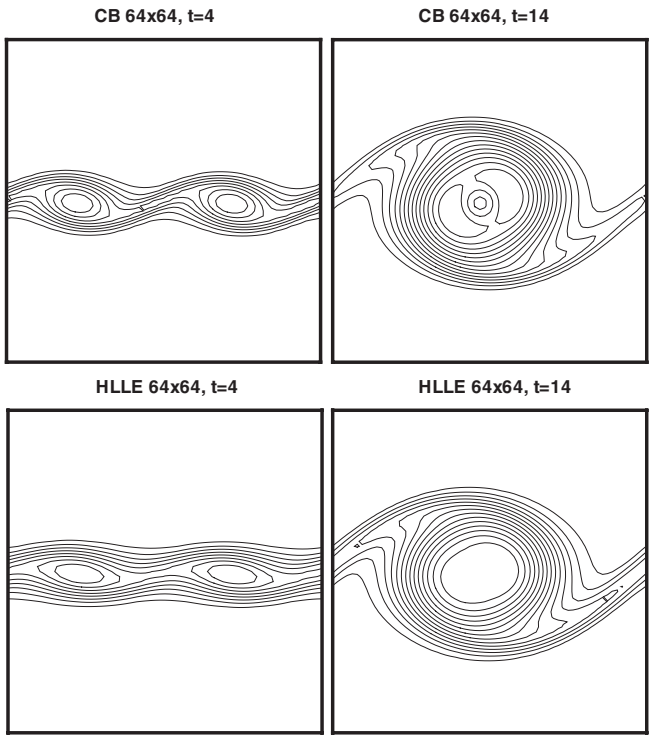

Figure 5. Isovorticity contours on the 64×64 grid for the CB [16, 9] and HLLE [30] Godunov-type schemes.

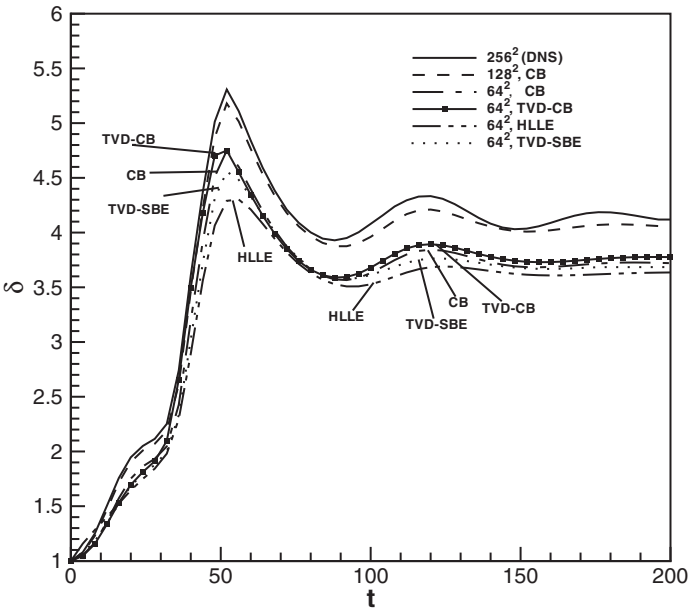

Figure 6. Growth of the vorticity thickness computed by different Godunov-type schemes; TVD-CB and TVD-SBE are the TVD versions of the CB scheme in conjunction with the CB and Superbee limiters, respectively. On the 256×256 grid, the results obtained by the CB and TVD-CB schemes are indistinguishable.

4. CONCLUDING REMARKS

TVD methods which have been developed for solving hyperbolic conservation laws encompass an embedded turbulence model which mimics properties of turbulence in a similar fashion with SGS models developed for LES. These methods essentially provide a non-linear numerical viscosity mechanism which is a function of the wave-speed dependent terms and flux limiters.

In this paper different Godunov-type schemes were utilized in computations of Burgers' turbulence and a two-dimensional mixing layer. The schemes included a TVD Godunov-type scheme developed here using the concept of flux limiters. The computations were conducted with and without SGS models. The accuracy depends on both the Godunov-type scheme and the SGS model. The TVD Godunov-type scheme provided the best results without use of a SGS model. Even though a theory that justifies the use of TVD methods as a turbulence modelling approach has not yet been developed, the present results show that these methods can be utilized in turbulent flow computations without SGS models.

Numerical challenges arising from the presence of wall boundaries will be addressed in a future work. Our end target is to develop numerical methods for turbulent flows which can attain increased accuracy in coarsely resolved computations.

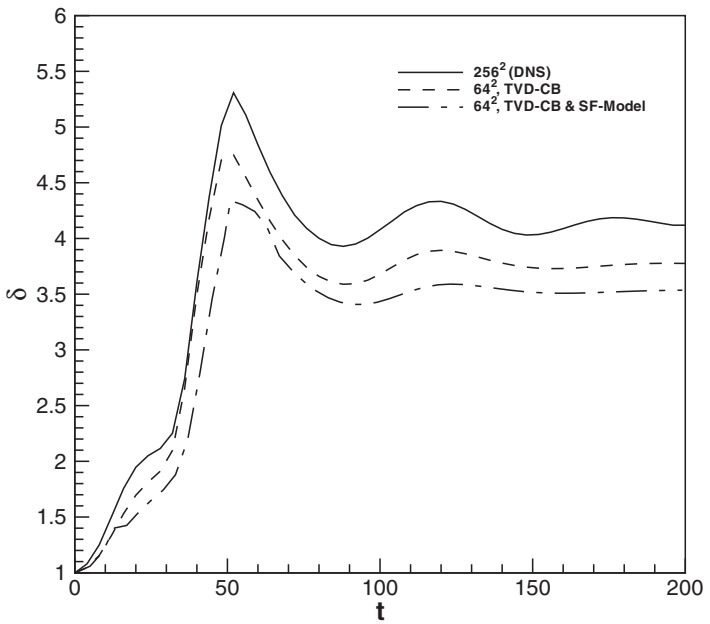

Figure 7. Comparison of the solutions obtained by the TVD-CB scheme with and without the structure-function SGS model; the solutions are labelled 'TVD-CB & SF-Model' and 'TVD-CB', respectively.

Table II. Multigrid (MG) cycles required by different Godunov-type schemes for completing 50 time steps (corresponding to dimensionless $t = 200$).

Method	MG cycles
CB, 256^2	334
CB, 128^2	663
CB, 64^2	883
TVD-CB, 64^2	353
HLLE, 64^2	531

APPENDIX A: COEFFICIENTS FOR THE SECOND-ORDER CB SCHEME FOR THE LINEAR ADVECTION EQUATION

The second-order Runge–Kutta discretization of the linear advection equation yields

$$\begin{aligned} K_1 &= -\Delta t \ f_x(t^n, u^n) \\ K_2 &= -\Delta t \ f_x(t^n + \Delta t, u^n + K_1) \\ u^{n+1} &= u^n + \frac{1}{2}(K_1 + K_2) \end{aligned} \tag{45}$$

Implementation of the CB flux (Equation (14)) gives

$$K_1 = b_{-2}u_{i-2}^n + b_{-1}u_{i-1}^n + b_0u_i^n + b_1u_{i+1}^n + b_2u_{i+2}^n \tag{46}$$

$$\begin{aligned} K_2 = {} & b_{-2}^2u_{i-4}^n + b_{-2}b_{-1}u_{i-3}^n + b_{-2}(1+b_0)u_{i-2}^n + b_{-2}b_1u_{i-1}^n + b_{-2}b_2u_i^n \\ & b_{-1}b_{-2}u_{i-3}^n + b_{-1}^2u_{i-2}^n + b_{-1}(1+b_0)u_{i-1}^n + b_{-1}b_1u_i^n + b_{-1}b_2u_{i+1}^n \\ & b_0b_{-2}u_{i-2}^n + b_0b_{-1}u_{i-1}^n + b_0(1+b_0)u_i^n + b_0b_1u_{i+1}^n + b_0b_2u_{i+2}^n \\ & b_1b_{-2}u_{i-1}^n + b_1b_{-1}u_i^n + b_1(1+b_0)u_{i+1}^n + b_1^2u_{i+2}^n + b_1b_2u_{i+3}^n \\ & b_2b_{-2}u_i^n + b_2b_{-1}u_{i+1}^n + b_2(1+b_0)u_{i+2}^n + b_2b_1u_{i+3}^n + b_2^2u_{i+4}^n \end{aligned} \tag{47}$$

where

$$\begin{aligned} b_{-2} &= -\frac{\mathscr{C}}{12}(1+s); \quad b_{-1} = \frac{\mathscr{C}}{12}(8+4s) \\ b_0 &= -\frac{\mathscr{C}}{2}s; \quad b_1 = -\frac{\mathscr{C}}{12}(8-4s); \quad b_2 = \frac{\mathscr{C}}{12}(1-s) \end{aligned} \tag{48}$$

Using Equations (46) and (47), Equation (45) yields

$$\begin{aligned} u_i^{n+1} = {} & c_{-4}u_{i-4}^n + c_{-3}u_{i-3}^n + c_{-2}u_{i-2}^n + c_{-1}u_{i-1}^n \\ & + c_0u_i^n + c_1u_{i+1}^n + c_2u_{i+2}^n + c_3u_{i+3}^n + c_4u_{i+4}^n \end{aligned} \tag{49}$$

where

$$\begin{aligned} c_{-4} &= \tfrac{1}{2}b_{-2}^2 \\ c_{-3} &= b_{-2}b_{-1} \\ c_{-2} &= \tfrac{1}{2}(2b_0b_{-2} + 2b_{-2} + b_{-1}^2) \\ c_{-1} &= b_1b_{-2} + b_0b_{-1} + b_{-1} \\ c_0 &= \tfrac{1}{2}(2b_2b_{-2} + 2b_1b_{-1} + b_0^2 + 2b_0) + 1 \\ c_1 &= b_2b_{-1} + b_0b_1 + b_1 \\ c_2 &= \tfrac{1}{2}(2b_0b_2 + 2b_2 + b_1^2) \\ c_3 &= b_2b_1 \\ c_4 &= \tfrac{1}{2}b_2^2 \end{aligned} \tag{50}$$

The coefficients (Equation (50)) satisfy Equation (13) for second-order of accuracy.

APPENDIX B: EINFELDT'S HLLE SCHEME [30]

The HLLE scheme [30] is an extension of the Harten–Lax–van Leer (HLL) scheme [34]. The central idea of the HLL scheme is to assume a particular wave configuration for the solution,

consisting of two waves separating three constant states. Assuming that the wave speeds are defined through a given algorithm, one can apply the integral form of the conservation laws and obtain an approximate expression for the flux. The difference between the original HLL scheme [34] and its HLLE version lies on the way the wave speeds are calculated. According to HLLE scheme the flux E is defined by

$$E_{i+1/2} = \frac{b^+_{i+1/2}E_L - b^-_{i+1/2}E_R}{b^+_{i+1/2} - b^-_{i+1/2}} + \frac{b^+_{i+1/2}b^-_{i+1/2}}{b^+_{i+1/2} - b^-_{i+1/2}}(U_R - U_L) \tag{51}$$

where $b^+_{i+1/2} = \max((\lambda_1)_i, (\lambda_1)_{i+1})$ and $b^-_{i+1/2} = \min((\lambda_2)_i, (\lambda_2)_{i+1})$. Implementation of the HLLE scheme in incompressible flows is also discussed in Reference [35].

ACKNOWLEDGEMENTS

Stimulating discussions with W. J. Rider, E. F. Toro, B. J. Geurts and P. K. Smolarkiewicz are gratefully acknowledged.

REFERENCES

1. Oran ES, Boris JP. Computing turbulent shear flows—A convenient conspiracy. *Computers in Physics* 1993; **7**:523–533.
2. Margolin LG, Smolarkiewicz PK, Sorbjan Z. Large-eddy simulations of convective boundary-layers using non-oscillatory differencing. *Physica D* 1999; **133**:390–397.
3. Margolin LG, Rider WJ. A rationale for implicit turbulence modeling. *CD-Rom ECCOMAS Proceedings*, ECCOMAS CFD Conference, Swansea, September 2001.
4. Rider WJ, Drikakis D. High resolution methods for computing turbulent flows. *Turbulent Flow Computation*. Kluwer Academic Publishers: (eds. D. Drikakis, B.J. Geurts), 43–74 (2002).
5. Smolarkiewicz PK, Prusa JM. Forward-in-time differencing for fluids: Simulation of geophysical turbulence. *Turbulent Flow Computation*. Kluwer Academic Publishers: (eds. D. Drikakis, B.J. Geurts), 279–312, (2002).
6. Porter DH, Pouquet A, Woodward PR. Kolmogorov-like spectra in decaying three-dimensional supersonic flows. *Physics of Fluids* 1994; **6**:2133–2142.
7. Brown AR, MacVean MK, Mason PJ. The effects of numerical dissipation in large eddy simulations. *Monthly Weather Review* 2000; **57**:3337–3348.
8. Thuburn J. Dissipation and cascade to small scales in numerical models using a shape-preserving advection scheme. *Monthly Weather Review* 1995; **123**:1888–1903.
9. Drikakis D. Uniformly high-order methods for unsteady incompressible flows. *Godunov Methods*: *Theory and Applications*. Kluwer Academic Publishers: (ed. E.F. Toro) 263–283, 2001.
10. Harten A. High resolution schemes for hyperbolic conservation laws. *Journal of Computational Physics* 1983; **49**:357–393.
11. Godunov SK. A finite difference method for the computation of discontinuous solutions of the equations of fluid dynamics. *Mat. Sb.* 1959; **47**:357–393.
12. Toro EF. *Riemann Solvers and Numerical Methods for Fluid Dynamics*. Springer-Verlag, 1999.
13. Boris JP, Book DL. Flux-corrected transport III: minimal-error FCT algorithms. *Journal of Computational Physics* 1976; **20**:397–431.
14. Sweby PK. High resolution schemes using flux limiters for hyperbolic conservation laws. *SIAM Journal of Numerical Analysis* 1984; **21**:995–1011.
15. Roe PL. Some contribution to the modelling of discontinuous flows. *In Proceedings of the SIAM/AMS Seminar*, San Diego, 1983.
16. Drikakis D, Govatsos PA, Papantonis DE. A characteristic-based method for incompressible flows. *International Journal for Numerical Methods in Fluids* 1994; **19**:667–685.
17. Kraichnan RH. Lagrangian-history statistical theory for Burgers' equation. *Physics of Fluids* 1968; **11**:265–277.
18. Lilly DK. A proposed modification of the Germano subgrid-scale closure method. *Physics of Fluids* 1992; **4**(3): 633–635.
19. Germano M, Piomelli U, Moin P, Cabot WH. A dynamic subgrid-scale eddy viscosity model. *Physics of Fluids* 1991; **3**(7):1760–1765.

20. Métais O, Lesieur M. Spectral large-eddy simulations of isotropic and stably-stratified turbulence. *Journal of Fluid Mechanics* 1992; **239**:157–194.
21. Chorin AJ. A numerical method for solving incompressible viscous flow problems. *Journal of Computational Physics* 1967; **2**:12–26.
22. Soh WY, Goodrich JW, Unsteady solution of incompressible Navier–Stokes equations. *Journal of Computational Physics* 1988; **79**:113–134.
23. Rogers SE, Kwak D, Kiris C. Steady and unsteady solutions of the incompressible Navier–Stokes equations. *AIAA Journal* 1991; **29**(4):603–610.
24. Shu C-W, Osher S. Efficient implementation of essentially non-oscillatory shock-capturing schemes. *Journal of Computational Physics* 1988; **77**:439–471.
25. Drikakis D, Iliev OP, Vassileva DP. A nonlinear multigrid method for the three-dimensional incompressible Navier–Stokes equations. *Journal of Computational Physics* 1998; **146**:310–321.
26. Roe PL. Numerical algorithms for the linear wave equation. Technical Report 81047, Royal Aircraft Establishment, Bedford, UK, 1981.
27. Lax PD. Weak solutions of nonlinear hyperbolic equations and their numerical computation. *Communications in Pure and Applied Mathematics* 1954; **VII**:159–193.
28. Thuburn J. TVD schemes, positive schemes, and the universal limiter. *Monthly Weather Review* 1990; **125**: 1990–1993.
29. Leonard A. Energy cascade in large-eddy simulations of turbulent fluid flow. *Advance in Geophysics* 1974; **18a**:237–248.
30. Einfeldt B. On Godunov-type methods for gas dynamics. *SIAM Journal of Numerical Analysis* 1988; **25**(2): 294–318.
31. Vreman B, Geurts B, Kuerten H. Discretization error dominance over subgrid terms in Large Eddy Simulation of compressible shear layers in 2D. *International Journal for Numerical Methods in Engineering* 1994; **10**: 785–790.
32. Lesieur M, Staquet C, Roy PL, Comte P. The mixing layer and its coherence examined from the point of view of two-dimensional turbulence. *Journal of Fluid Mechanics* 1988; **192**:511–534.
33. Michalke A. On the inviscid instability of the hyperbolic tangent velocity profile. *Journal of Fluid Mechanics* 1964; **19**:543–556.
34. Harten A, Lax P, van Leer B. On upstream differencing and Godunov-type schemes for hyperbolic conservation laws. *SIAM Review* 1983; **25**:35–61.
35. Drikakis D, Smolarkiewicz PK. On spurious vortical structures. *Journal of Computational Physics* 2001; **172**: 309–325.

